Computer methods in applied mechanics and engineering

ELSEVIER Comput. Methods Appl. Mech. Engrg. 190 (2001) 4663–4675

www.elsevier.com/locate/cma

Averaging technique for FE – a posteriori error control in elasticity. Part II: λ-independent estimates

Carsten Carstensen, Stefan A. Funken *

Universitat Kiel, Mathematics Seminar, Ludewig-Meyn-Strasse 4, 24098 Kiel, Germany

Received 22 February 2000

Abstract

In the second part of our investigation on a posteriori error estimates and a posteriori error control in finite element analysis in elasticity, we focus on robust a posteriori error bounds. First we establish a residual-based a posteriori error estimate which is reliable and efficient up to higher-order terms and λ-independent multiplicative constants; the Lamé constant λ steers the incompressibility. Second we show the robust efficiency and reliability of averaging techniques in certain norms. Numerical evidence supports that the reliability of depends on the smoothness of given right-hand sides and is independent of the structure of a shape-regular mesh. © 2001 Elsevier Science B.V. All rights reserved.

MSC: 65N30; 65R20; 73C50

Keywords: Elasticity; A posteriori error estimates; Adaptive algorithm; Reliability; Finite element method; Locking

1. Introduction

Error control and efficient mesh-design in finite element simulations of computational engineering and scientific computing are frequently based on a posteriori error estimates [1,11,14–16], where the question of nearly incompressible material and locking phenomena is usually excluded. For a Poisson ratio v close to 1/2, the Lamè constant λ is very large and dominates in the Navier–Lamè equations

$$(\lambda + \mu)\nabla \operatorname{div} u + \mu\Delta u = -f. \tag{1.1}$$

The second part of our investigation [6,7] on efficient and reliable averaging techniques in a posteriori error control shows that the constants c_1 and c_2 in the estimate

$$E/c_1 \leqslant \eta \leqslant c_2 E + \text{h.o.t.} \tag{1.2}$$

for the error E and the computable a posteriori error bound η are independent of the meshsize and the parameter λ. In (1.2), the error norm is ($||\cdot||_{L^2(\Omega)}$ denotes the $L^2(\Omega)$-norm)

$$E = ||2\mu\varepsilon(u - u_h)||_{L^2(\Omega)} + ||\lambda \operatorname{div}(u - u_h)||_{L^2(\Omega)} \tag{1.3}$$

* Corresponding author.

E-mail addresses: cc@numerik.uni-kiel.de (C. Carstensen), saf@numerik.uni-kiel.de (S.A. Funken).

PII: S 0 0 4 5 - 7 8 2 5 (0 0) 0 0 3 3 8 - 8

and the error estimator for the residual-based a posteriori error estimate reads

$$\eta = ||h_{\mathscr{T}}(f + \mathrm{div}_{\mathscr{T}}\sigma_h)||_{L^2(\Omega)} + ||h_{\mathscr{E}}^{1/2}[\sigma_h]n_{\mathscr{E}}||_{L^2(\cup\mathscr{E})}, \tag{1.4}$$

where $h_{\mathscr{T}}$ and $h_{\mathscr{E}}$ denote the element size and edge size, σ_h is the discrete stress with elementwise divergence $\mathrm{div}_{\mathscr{T}}$ and edgewise jump of the normal components $[\sigma_h]n_{\mathscr{E}}$ on the union of all edges $\cup\mathscr{E}$ (the skeleton of all element boundaries). The arguments in [4,5,9] allow a refined estimate that states that the edge contributions dominate, i.e., (1.2) holds for (1.3) and

$$\eta = ||h_{\mathscr{E}}^{1/2}[\sigma_h]||_{L^2(\cup\mathscr{E}))} + \text{h.o.t.} \tag{1.5}$$

The final result states that any averaging technique is reliable, e.g., that (1.2) holds for (1.3) and

$$\eta = \min_{\sigma^*\in\mathscr{Q}(\mathscr{T},g)} ||\sigma_h - \sigma^*||_{L^2(\Omega)} + \text{h.o.t.}, \tag{1.6}$$

where $\mathscr{Q}(\mathscr{T},g)$ denotes the globally continuous and piecewise affine splines which satisfy Neumann boundary conditions.

The Part II in this series on averaging techniques provides robust error control for a finite element discretisation of (1.1) in the sense that λ (explicitly arising in the error norm E as well as in the error estimator η) does not affect the constants c_1 and c_2 in (1.2). We study the influence of the approximation of mixed inhomogeneous boundary conditions and the higher-order terms (h.o.t.).

The outline of the paper is as follows. The model problem and precise descriptions of material properties and the regularity of right-hand sides are given in Section 2 together with precise statements of (1.2)–(1.6) that include the proper treatment of boundary conditions. Algorithms are described in Section 3. Numerical evidence is provided in Section 4 and shows almost asymptotic exactness of our realisation of the ZZ-estimator for adapted meshes when we start with a structured grid. For more unstructured perturbed grids, the reliability and efficiency are still observed with very good constants. The proofs are given in Section 5 following arguments in [5,6,8]. It should be stressed that the error norm E in (1.3) is *not* the energy norm and indeed, the authors tried and failed to prove the reliability for the ZZ-estimator in the energy norm (cf. [6, Section 6 in Part I] for a heuristic). Nevertheless, numerical examples indicate that the energy-norm version of the ZZ-estimator performs well.

In Part III of this series [7], we investigate non-conforming schemes which are locking-free and we will provide robust reliable and efficient averaging techniques for their practical realisation.

2. Model example and results

The stress field σ satisfies the equilibrium equations

$$f + \mathrm{div}\,\sigma = 0 \quad \text{in } \Omega, \tag{2.1}$$

$$\sigma \cdot n = g \quad \text{on } \Gamma_{\mathrm{N}} \tag{2.2}$$

for given volume force $f \in L^2(\Omega)^d$ and applied surface load $g \in L^2(\Gamma_{\mathrm{N}})^d$. The Lipschitz boundary $\Gamma = \partial\Omega$ of the body, occupied by a bounded domain Ω in $\mathbb{R}^d$, consists of a closed Dirichlet part Γ_{D} with positive surface measure and a remaining, relatively open and possibly empty, Neumann part $\Gamma_{\mathrm{N}} := \Gamma \setminus \Gamma_{\mathrm{D}}$.

The Dirichlet data $u_{\mathrm{D}} \in C(\Gamma_{\mathrm{D}})$ are supposed to be differentiable at any flat piece of Γ_{D} such that the surface gradient is square-integrable (written $u_{\mathrm{D}} \in H^1(\Gamma_{\mathrm{D}})$). Then, we suppose that the exact displacement field u belongs to $H^1(\Omega)^d$, i.e., $u \in L^2(\Omega)^d$ and the gradient Du is an $L^2(\Omega)^{d\times d}$-function, and satisfies

$$u = u_{\mathrm{D}} \quad \text{on } \Gamma_{\mathrm{D}}. \tag{2.3}$$

The linear Green strain tensor $\varepsilon(u) := \mathrm{sym}\,Du = (1/2)(u_{j,k} + u_{k,j})_{j,k=1}^d$ is linearly related to the stress σ

$$\sigma = \mathbb{C}_{\varepsilon}(u) \quad \text{in } \Omega. \tag{2.4}$$

The two positive Lamè constants λ and μ play different roles in the material law

$$\mathbb{C}_{\mathscr{T}} = \lambda\,\mathrm{tr}\,(\mathscr{T})\mathbb{1} + 2\mu\mathscr{T} \quad \text{for all } \mathscr{T} \in \mathbb{R}^{d\times d}_{\mathrm{sym}}, \tag{2.5}$$

where tr denotes the trace of a matrix and $\mathbb{1}$ is the unit matrix. While μ is fixed we carefully analyse $\lambda \to \infty$ in the material law (2.5) and denote the dependence of λ explicitly in the notation.

There exists exactly one (weak) solution $u \in H^1(\Omega)^d$ to (2.1)–(2.4). (The Lebesgue and Sobolev spaces $L^2(\Omega)$ and $H^1(\Omega)$ are defined as usual [12,13].) The unknown exact solution u is approximated by a finite element method on a mesh $\mathscr{T}$. We suppose that $\mathscr{T}$ is a regular triangulation of $\Omega \subset \mathbb{R}^d$ in the sense of Ciarlet [10], i.e., $\mathscr{T}$ is a finite partition of Ω into closed triangles or parallelograms if $d = 2$ and tetrahedrons if $d = 3$. We suppose that two distinct elements T_1 and T_2 in $\mathscr{T}$ are either disjoint or $T_1 \cap T_2$ is a complete face, a common edge or a common node of both T_1 and T_2. With $\mathscr{T}$ let $\mathscr{N}$ denote the set of all nodes and let $\mathscr{E}$ denote the set of all faces if $d = 3$ and an edge if $d = 2$. For simplicity, we call $E \in \mathscr{E}$ an edge (even if $d = 3$ and E is a face) and we assume that $E \in \mathscr{E}$ either belongs to Γ_{D} or $E \cap \Gamma_{\mathrm{D}}$ has vanishing surface measure, so there is no change of boundary conditions within one edge $E \subseteq \Gamma$. Furthermore, let $P_k(T)$, resp. $Q_k(T)$, denote the set of the algebraic polynomials of total, resp. partial, degree $\leqslant k$ and define $\mathscr{P}_k(T) := P_k(T)$ if T is a triangle or tetrahedron and $\mathscr{P}_k(T) := Q_k(T)$ if T is a parallelogram.

Then the finite element methods provide a discrete solution u_h which belongs to $\mathscr{S}$,

$$\mathscr{S} := \mathscr{S}_1(\mathscr{T})^d := \{v_h \in C(\Omega)^d : \forall T \in \mathscr{T}, v_h|_T \in \mathscr{P}_1(T)\} \tag{2.6}$$

and satisfy, for all test functions $v_h \in \mathscr{S}_{\mathrm{D}} := \{v_h \in \mathscr{S} : v_h = 0 \text{ on } \Gamma_{\mathrm{D}}\}$, with homogeneous Dirichlet conditions, the discrete weak form of equilibrium

$$\int_\Omega \varepsilon(v_h) : \mathbb{C}_\varepsilon(u_h)\,\mathrm{d}x = \int_\Omega f \cdot v_h\,\mathrm{d}x + \int_{\Gamma_{\mathrm{N}}} g \cdot v_h\,\mathrm{d}s. \tag{2.7}$$

In case of pure Dirichlet conditions $\Gamma = \Gamma_{\mathrm{D}}$ we require

$$\int_\Gamma (u_{\mathrm{D}} - u_h) \cdot n\,\mathrm{d}s = 0 \tag{2.8}$$

(while there is no such further condition if Γ_{N} has a positive surface measure). To assess the error in the geometric boundary conditions, we define the abstract error term

$$\eta_{\mathrm{D}} := \inf\,\{||\varepsilon_{\mathscr{T}}(u_h - \eta)||_{L^2(\Omega)} : \eta \in H^1(\Omega)^d, \eta = u_{\mathrm{D}} \quad \text{on } \Gamma_{\mathrm{D}}\}. \tag{2.9}$$

The infimum in (2.9) is attained (so we could replace inf by min therein) and can be estimated in case the boundary approximation of u_h is specified (cf. Remark 2.1 below for a brief discussion).

The discrete stress jumps $[\sigma_h]n_{\mathscr{E}}$ on the skeleton $\cup\mathscr{E}$ are defined along the edge $E \in \mathscr{E}$ as $[\sigma_h]n_{\mathscr{E}} = 0$ if $E \subset \Gamma_{\mathrm{D}}$, as $[\sigma_h]n_{\mathscr{E}} = (\sigma_h|_{T_+} - \sigma_h|_{T_-})n_{\mathscr{E}})$ on an interior edge $T_+ \cap T_- = E, T_\pm \in \mathscr{T}$, and $[\sigma_h]n_{\mathscr{E}} = g - \sigma_h n$ on $E \subset \bar{\Gamma}_{\mathrm{N}}$.

The standard residual-based a posteriori error estimate has the following new robust variant (proofs will be given in Section 5). The subsequent result is a precise statement of the upper bound in (1.2) for the estimator (1.4).

Theorem 2.1. *Let $u \in H^1(\Omega)^d$ solve (2.1)–(2.4) and let $u_h \in \mathscr{S}$ satisfy (2.7). Suppose $f \in L^2(\Omega)^d$ and $g \in L^2(\Gamma_{\mathrm{N}})$. Then*

$$||2\mu\varepsilon(u - u_h)||_{L^2(\Omega)} + ||\lambda\,\mathrm{div}(u - u_h)||_{L^2(\Omega)} \leqslant c_3\Big(||h_{\mathscr{T}}(f + \mathrm{div}_{\mathscr{T}}\sigma_h)||_{L^2(\Omega)} + ||h_{\mathscr{E}}^{1/2}[\sigma_h]n_{\mathscr{E}}||_{L^2(\cup\mathscr{E})} + \eta_{\mathrm{D}}\Big). \tag{2.10}$$

The $(h_{\mathscr{T}}, h_{\mathscr{E}}, \lambda)$-independent constant $c_3 > 0$ depends on the shape of the elements and patches only.

The refinement concerns the volume contribution $||h_{\mathscr{T}}(f + \mathrm{div}_{\mathscr{T}}\sigma_h)||_{L^2(\Omega)}$ which can be replaced by a higher-order term as in the estimator (1.5).

Theorem 2.2. *Let $u \in H^1(\Omega)^d$ solve* (2.1)–(2.4) *and let $u_h \in \mathscr{S}^1(\mathscr{T})^d$ satisfy* (2.7). *Suppose $f \in H^1(\Omega)^d$ and $g \in L^3(\Gamma_{\mathrm{N}})$. Then*

$$||2\mu\varepsilon(u-u_h)||_{L^2(\Omega)} + ||\lambda\,\mathrm{div}(u-u_h)||_{L^2(\Omega)} \leqslant c_3\Big(||h_{\mathscr{E}}^{1/2}[\sigma_h]n_{\mathscr{E}}||_{L^2(\cup\mathscr{E})} + ||h_{\mathscr{T}}^2\nabla f||_{L^2(\Omega)} + \eta_{\mathrm{D}}\Big). \tag{2.11}$$

The $(h_{\mathscr{T}}, h_{\mathscr{E}}, \lambda)$-independent constant $c_4 > 0$ depends on the shape of the elements and patches only.

The efficiency of the error estimators in (2.10) resp. (2.11) was shown by Verfürth in [15] whence we state the theorem and do not recall the proof of the first inequality in (1.2).

Theorem 2.3. *Let $u \in H^1(\Omega)^d$ solve* (2.1)–(2.4) *and let $u_h \in \mathscr{S}$* satisfy (2.7). *Suppose $f \in H^1(\Omega)^d$ and $g \in H^1(\Gamma_{\mathrm{N}})$, and $u_{\mathrm{D}} \in H^2(\Gamma_{\mathrm{D}})$. Then*

$$\begin{aligned}||h_{\mathscr{T}}(f+\mathrm{div}_{\mathscr{T}}\sigma_h)||_{L^2(\Omega)} + ||h_{\mathscr{E}}^{1/2}[\sigma_h]n_{\mathscr{E}}||_{L^2(\cup\mathscr{E})} &\leqslant c_5\Big(||2\mu\varepsilon(u-u_h)||_{L^2(\Omega)} + ||\lambda\,\mathrm{div}(u-u_h)||_{L^2(\Omega)}\\ &+ ||h_{\mathscr{E}}^{3/2}\partial^2 u_{\mathrm{D}}/\partial s^2||_{L^2(\Gamma_{\mathrm{D}})} + ||h_{\mathscr{E}}^{3/2}\partial g/\partial s||_{L^2(\Gamma_{\mathrm{N}})} + ||h_{\mathscr{T}}^2\nabla f||_{L^2(\Omega)}\Big).\end{aligned} \tag{2.12}$$

The $(h_{\mathscr{T}}, h_{\mathscr{E}}, \lambda)$-independent constant $c_5 > 0$ depends on the shape of the elements and patches only.

The final part concerns averaging techniques where we have robust reliable and efficient error control. Recall from Part I [6] that, with $\mathscr{E}_{\mathrm{N}}$ denoting the edges on the Neumann boundary,

$$\mathscr{Q}(\mathscr{T},g) := \{\sigma_h^* \in \mathscr{S}^1(\mathscr{T})^{d\times d} : \sigma_h^*(z)\cdot n_E = g(z) \quad \text{for all } z \in \mathscr{N}\cap E \quad \text{with} \quad E \in \mathscr{E}_N\} \tag{2.13}$$

which requires some continuity on g: At those nodes z on Γ_{N} where Γ_{N} is flat and so the normal vectors coincide $n_{E_1} = n_{E_2}$ for two distinct neighbouring $E_1, E_2, \in \mathscr{E}_{\mathrm{N}}$, the continuity of σ_h^* at $z \in E_1\cap E_2\cap\mathscr{N}$ implies that the restrictions $g|_{E_1}$ and $g|_{E_2}$ coincide at z. Note that $\mathscr{Q}(\mathscr{T},g) = \mathscr{S}^1(\mathscr{T})^{d\times d}$ in the case of pure Dirichlet conditions. Then

$$\eta_Z := \min_{\sigma_h^*\in\mathscr{Q}(\mathscr{T},g)} ||\sigma_h - \sigma_h^*||_{L^2(\Omega)} \tag{2.14}$$

is a lower bound of each averaging estimator (up to the Neumann boundary conditions). The subsequent result implies (1.2) for the estimator (1.6).

Theorem 2.4. *Let $u \in H^1(\Omega)^d$ solve* (2.1)–(2.4) *and let $u_h \in \mathscr{S}^1(\mathscr{T})^d$ satisfy* (2.7). *Suppose $f \in H^1(\Omega)^d$ and $g \in H^2(\mathscr{E}_{\mathrm{N}})$, i.e, $g|_E \in H^2(E)^d$ for all $E \in \mathscr{E}$ with $E \subset \overline{\Gamma}_{\mathrm{N}}$. Then*

$$\begin{aligned}\eta_Z - \min_{\sigma_h^*\in\mathscr{Q}(\mathscr{T},g)} ||\sigma - \sigma_h^*||_{L^2(\Omega)} &\leqslant ||2\mu\varepsilon(u-u_h)||_{L^2(\Omega)} + ||\lambda\,\mathrm{div}(u-u_h)||_{L^2(\Omega)}\\ &\leqslant c_6\Big(\eta_Z + ||h_{\mathscr{T}}^2\nabla f||_{L^2(\Omega)} + \eta_{\mathrm{D}} + ||h_{\mathscr{E}}^{3/2}\partial_{\mathscr{E}} g/\partial s||_{L^2(\Gamma_N)}\Big).\end{aligned} \tag{2.15}$$

The $(h_{\mathscr{T}}, h_{\mathscr{E}}, \lambda)$-independent constant $c_6 > 0$ depends on the shape of the elements and patches only.

Remark 2.1. The term η_{D} can be of higher order. For instance, if the geometric boundary conditions of u_h are satisfied in each node,

$$u_h(z) = u_{\mathrm{D}}(z) \qquad \text{for all nodes } z \in \mathscr{N}_{\mathrm{D}} := \mathscr{N}\cap\Gamma_{\mathrm{D}} \tag{2.16}$$

and the Dirichlet data $u_{\mathrm{D}} \in H^1(\Gamma_{\mathrm{D}})$ are $\mathscr{E}_{\mathrm{D}}$-piecewise smooth, e.g., $u_{\mathrm{D}}|_E \in H^2(\mathscr{E})$ for all $E \in \mathscr{E}$ with $E \subset \Gamma_{\mathrm{D}}$, then

$$\eta_{\mathrm{D}} \leqslant c_7\Big\|h_{\mathscr{E}}^{1/2}\partial_{\mathscr{E}}(u_h - u_{\mathrm{D}})/\partial_s\Big\|_{L^2(\Gamma_{\mathrm{D}})} \leqslant c_7\Big\|h_{\mathscr{E}}^{3/2}\partial_{\mathscr{E}}^2 u_{\mathrm{D}}/\partial s^2\Big\|_{L^2(\Gamma_{\mathrm{D}})}, \tag{2.17}$$

where $h_{\mathscr{E}}$ denotes the local edge-length on $\cup\mathscr{E}$ and $\partial_{\mathscr{E}}(\cdot)/\partial s$ denotes the edgewise tangential derivative. The $h_{\mathscr{T}}$-independent constant c_7 is independent of u_{D} and depends only on the aspect ratio of the elements in $\mathscr{T}$.

(The estimate (2.17) is proved in [5] for $d = 2$, in [2] for $d = 3$.) In case of pure Dirichlet conditions, (2.16) is feasible in simple cases with the additional property (2.8). In general, (2.16) and (2.8) may not hold simultaneously.

3. Adaptive algorithms

The numerical examples provide experimental evidence of the efficiency, reliability and robustness of the a posteriori error estimate and illustrates the performance of adaptive algorithms.

Instead of η_Z we calculate $\eta_{\mathscr{A}} := ||\sigma_h - \mathscr{A}\sigma_h||_{L^2(\Omega)}$ with the averaging operator $\mathscr{A}$ based on a function $\sigma_h^* \in \mathscr{S}^1(\mathscr{T})^{2\times 2}$ which satisfies $g(z) = \sigma_h^*(z)n_E(z)$ for each endpoint z of an edge E on $\overline{\Gamma}_{\mathrm{N}}$. We define

$$\mathscr{A}\sigma_h := \sigma_h^* := \sum_{z\in\mathscr{N}} \mathscr{I}_z(\sigma_h)\varphi_z, \tag{3.1}$$

where, for $z \in \mathscr{N} \setminus \overline{\Gamma}_{\mathrm{N}}, \mathscr{I}_z(\sigma_h) := \fint_{\Omega_z} \sigma_h \, \mathrm{d}x$ is the integral mean of σ_h over Ω_z, For $z \in \mathscr{N} \cap \overline{\Gamma}_{\mathrm{N}}$ the discrete Neumann condition $g(z) = \sigma_h^*(z)n_E$ is included by solving 4×4 linear system of equations. We refer to Part I [6] for computational details.

The following algorithm generated all meshes of this paper and is explained with more details in Part I. We merely mention that some notations are defined therein $\vartheta = 1$ yields perturbed meshes for comparison to $\vartheta = 0$.

Algorithm ((A_A^ϑ), *resp.* (A_R^ϑ)).

(a) Start with a coarse mesh $\mathscr{T}_0, k = 0$.

(b) Solve the discrete problem with respect to the actual mesh $\mathscr{T}_k$ with N degrees of freedom and error $e_N := ||\sigma - \sigma_h||_{L^2(\Omega)}$.

(c) For Algorithm ($A_{\mathscr{A}}^\vartheta$) compute, for all $T \in \mathscr{T}_k$,

$$\eta_T = \eta_{\mathscr{A},T} := ||\sigma_h - \mathscr{A}\sigma_h||_{L^2(T)}.$$

For Algorithm (A_R^ϑ) compute, for all $T \in \mathscr{T}_k$ $\eta_T = \eta_{R,T}$ with

$$\eta_{R,T}^2 := ||f||_{L^2(T)}^2 + ||[\sigma_h \cdot n]||_{L^2(\partial T)}^2.$$

(d) Compute a given stopping criterion based on $\left(\sum_{T\in\mathscr{T}_k} \eta_T^2\right)^{1/2}$, denoted η_R, respectively, $\eta_{\mathscr{A}}$, and decide to terminate or go to (e).

(e) Mark the element T (*red* refinement) provided,

$$\frac{1}{2}\max_{T'\in\mathscr{T}_k} \eta_{\mathscr{T}'} \leqslant \eta_T.$$

(f) Mark further element (*red-green-blue*-refinement) to avoid hanging nodes. Generate a new triangulation $\widetilde{\mathscr{T}}_{k+1}$ using edge-midpoints if $\vartheta = 0$ and points on the edges at a random distance at most 0.3 h_E from the edge-midpoints if $\vartheta = 1$. Perturb the nodes $z \in \mathscr{N}_{k+1}$ of the mesh $\widetilde{\mathscr{T}}_{k+1}$ at random with values taken uniformly from a ball around z of radius $\vartheta 2^{-k}/15$. Correct boundary nodes by orthogonal projection onto that boundary piece they are expected such that Ω, Γ_{D}, Γ_{N} are matched by the resulting mesh $\mathscr{T}_{k+1}$ exactly. Update k and go to (b).

4. Numerical experiments

The three numerical experiments of Part I [6] are complemented in this section with L^2-stress-error norms e_N and corresponding estimators η_R and η_Z; notation is adopted from Algorithm (A_Z^ϑ), resp. (A_R^ϑ). All examples concern the Navier–Lamé equation (1.1) in the form of (2.1)–(2.6) and more details are reported in Part I [6, Sections 4.1–4.3].

4.1. L-shaped domain with analytic solution

The model example of the L-shaped domain with corners $(0,0)$, $(-1,-1)$ $(0,-2)$, $(2,0)$, $(0,2)$, and $(-1,1)$ models singularities at re-entrant corners for Young's modulus $E = 100,000$ and the Poisson coefficient $0.3 \leqslant \nu < 0.5$. The considered exact solution is traction free, $g = 0$, on the Neumann boundary $\Gamma_{\mathrm{N}} := \mathrm{conv}\{(0,0),(-1,1)\} \cup \mathrm{conv}\{(0,0),(-1,-1)\}$ and $f = 0$.

Starting from the initial mesh $\mathscr{T}_0$ from Fig. 1 (top, left), we run Algorithm $(A^0_{\mathscr{A}})$. The resulting mesh after 11 adaptive refinements and a zoom at the re-entrant corner is shown in Fig. 2 and displays a rather high mesh-refinement near the singularity.

Errors e_N and error estimators $\eta_{\mathscr{A}}$, η_R are displayed versus the number of degrees of freedom N for $\nu = 0.333$ and 0.499 for uniform meshes and adaptively refined meshes generated by Algorithms $(A^0_{\mathscr{A}})$, resp. (A^0_R) in Fig. 3. For the sequences of uniform meshes, we obtain experimentally convergence $\approx$0.54 which coincides with the theoretically expected rate. (Note, $N \propto h^{-2}$ in two dimensions.) Although the refined meshes $\mathscr{T}_1, \ldots, \mathscr{T}_k$ do not show the expected 'standard' refinement (circular around the origin) for $\mu = 0.499$, the adaptive mesh-refining Algorithm $(A^0_{\mathscr{A}})$ improves this experimental convergence order to 1 which is optimal for the used family of finite element spaces.

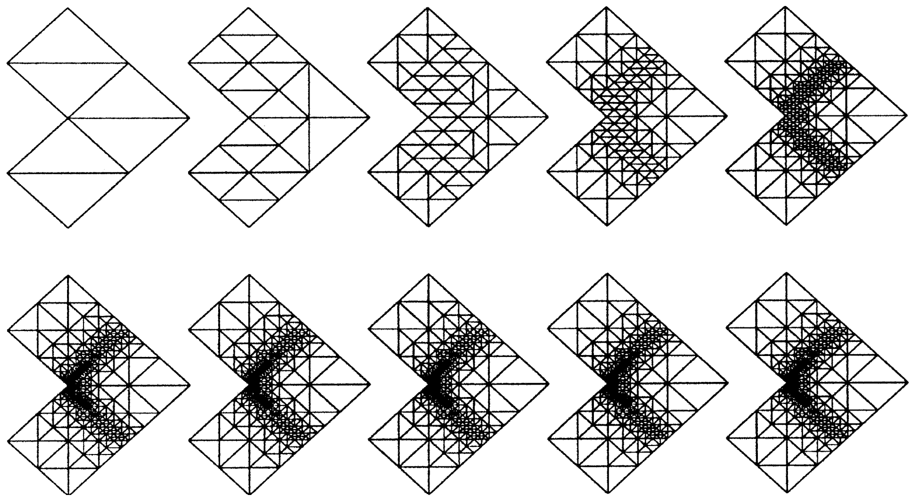

Fig. 1. $\mathscr{T}_0, \ldots, \mathscr{T}_9$ generated by Algorithm $(A^0_{\mathscr{A}})$ in Section 4.1 ($\nu = 0.4999$).

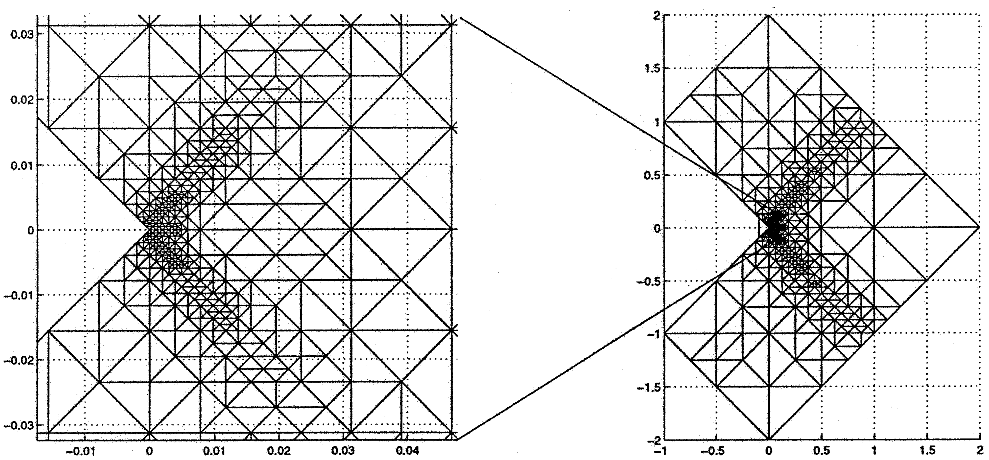

Fig. 2. Mesh $\mathscr{T}_{11}$ and magnified detail at the re-entrant corner for Section 4.1 ($\mu = 0.499$).

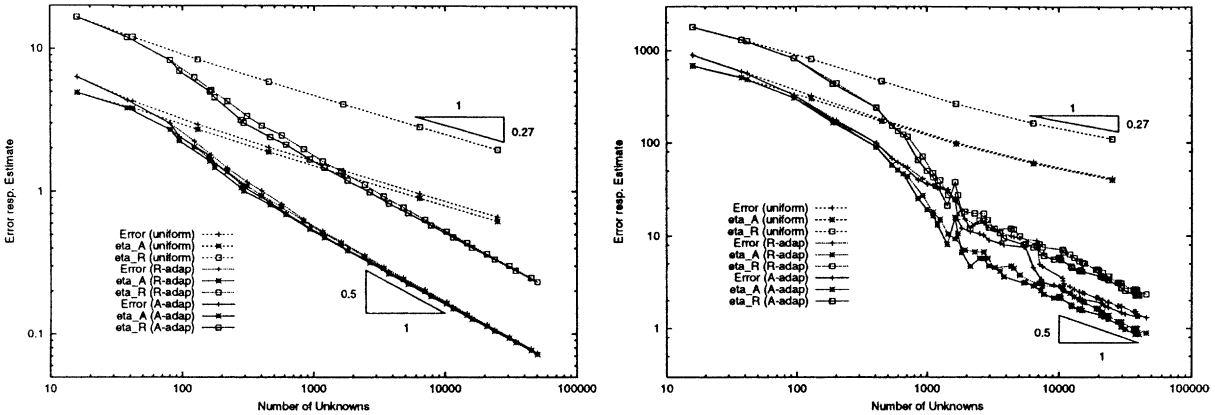

Fig. 3. Error indicators $\eta_{\mathscr{A}}$ and η_R vs N for uniform and adaptive meshes from Algorithm $(A^0_{\mathscr{A}})$ and $(A^0_{\mathscr{R}})$ of Section 4.1 ($\nu = 1/3$ left, $\nu = 0.499$ right).

The displacement formulation shows incompressibility locking phenomena in Fig. 3, i.e., the error in energy norm is not bounded (for a given number of unknowns) as $\nu \to 1/2$.

Super-convergence properties are frequently believed to be responsible for the good performance of averaging techniques for a posteriori error control in practice. We take Algorithm $(A^1_{\mathscr{A}})$ to study the influence of local symmetries in the mesh. Algorithm $(A^1_{\mathscr{A}})$ perturbs the nodes in step (f). (We refer to [6] for a figure of a sequence of perturbed refined meshes form Algorithm $(A^1_{\mathscr{A}})$.

For perturbed and non-perturbed meshes from Algorithm $(A^{\vartheta}_{\mathscr{A}})$, we display the extreme quotients of the error estimator $\eta_{\mathscr{A}}$ over the error $e_N = ||\sigma - \sigma_h||_{L^2(\Omega)}$ versus $1/2 - \nu$, i.e., the displayed constants are $\min\{\eta_A/e_N\}$, and $\max\{\eta_A/e_N\}$ for different values of N corresponding to $\mathscr{T}_1, \ldots, \mathscr{T}_k$ for k as implicitly shown in Fig. 1.

Fig. 4 shows that the reliability constant is bounded from above and the efficiency constant from below independently from the Poisson ratio ν. Ths numerical experiment confirms numerically that the a posteriori error estimate is h-independent and supports that also for perturbed meshes the estimate (2.15) is reliable and efficient.

4.2. Cook's membrane problem

A tapered panel is clamped on the left end as depicted in Fig. 5 subject to a shearing load on the right end, i.e., $g = (0, 1000)$ on the right edge of Ω, $g = 0$ on the remaining part of Γ_N, $u = 0$ on Γ_D and $f = 0$.

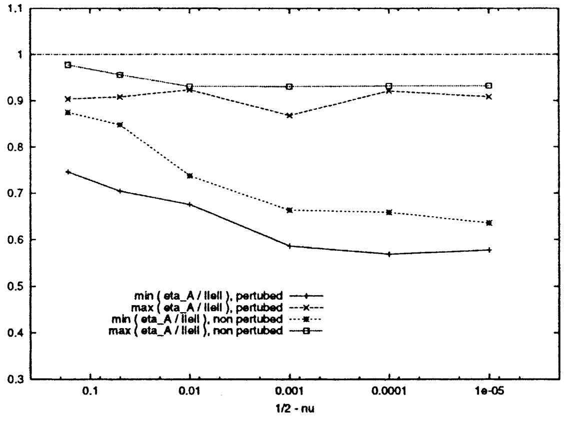

Fig. 4. Computed reliability/efficiency constants vs $1/2 - \nu$ for perturbed and non-perturbed meshes from Algorithm $(A^{\vartheta}_{\mathscr{A}})$ of Section 4.1.

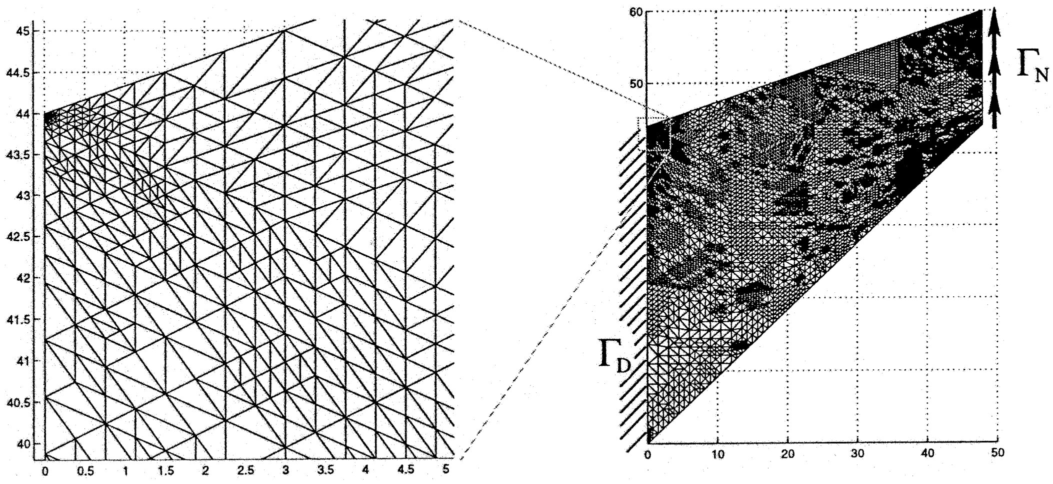

Fig. 5. Mesh $\mathcal{T}_{11}$ generated by Algorithm $(A^0_{\mathscr{A}})$ and magnified detail at $(0, 44)$ of Section 4.2 $(\nu = 1/3)$.

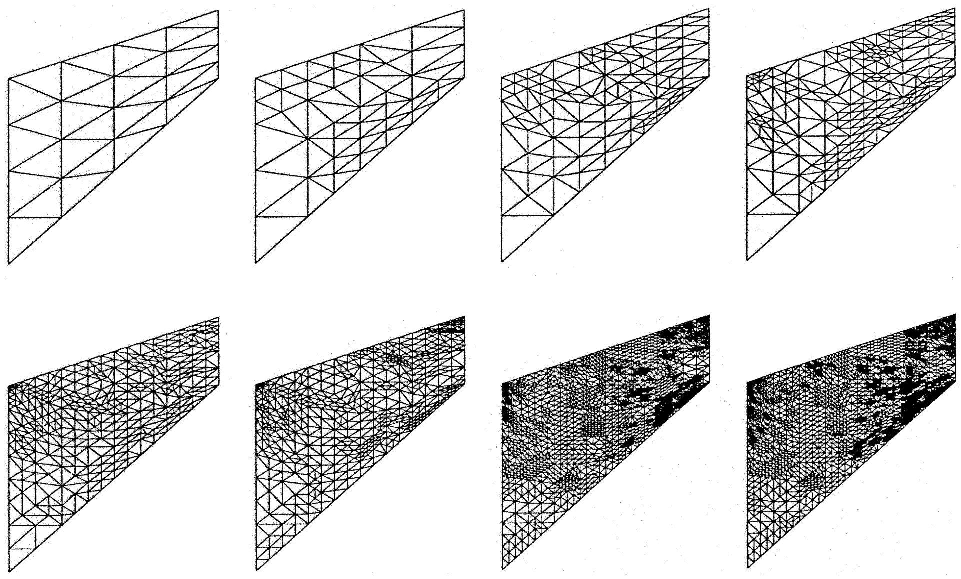

Fig. 6. $\mathcal{T}_0, \ldots, \mathcal{T}_7$ generated by Algorithm $(A^0_{\mathscr{A}})$ in Section 4.2 $(\nu = 1/3)$.

The material constants are $E = 100,000$ and $\nu = 1/3$ or 0.499 and the initial mesh $\mathcal{T}_0$ is displayed in Fig. 6 (top, left).

A plot of $\mathcal{T}_{11}$ generated by Algorithm $(A^0_{\mathscr{A}})$ as some magnified detail near the re-entrant corner (zoom of $(0, 5) \times (40, 45)$) is given in Fig. 5 for $\nu = 1/3$.

The a posteriori error estimates $\eta_{\mathscr{A}}$ and η_R for $\nu = 1/3$ (left) and $\nu = 0.499$ (right) computed with uniform and adaptive refinements are given in Fig. 7.

The adaptive mesh-refining Algorithms (A^0_Z) and (A^0_R) yield a slope $-1/2$. Assuming that the error estimator η_A is efficient and reliable as in Example 4.1 we obtain convergence order 1 which is asymptotically better than uniform refinement as observed in Fig. 7.

Since the exact solution is unknown for this example, we only show the a posteriori error estimate by η_R resp. $\eta_{\mathscr{A}}$. (Here, we consider the L^2-norm of $\sigma - \sigma_h$ which cannot be calculated by Galerkin-orthogonality as the energy norm in Part I.)

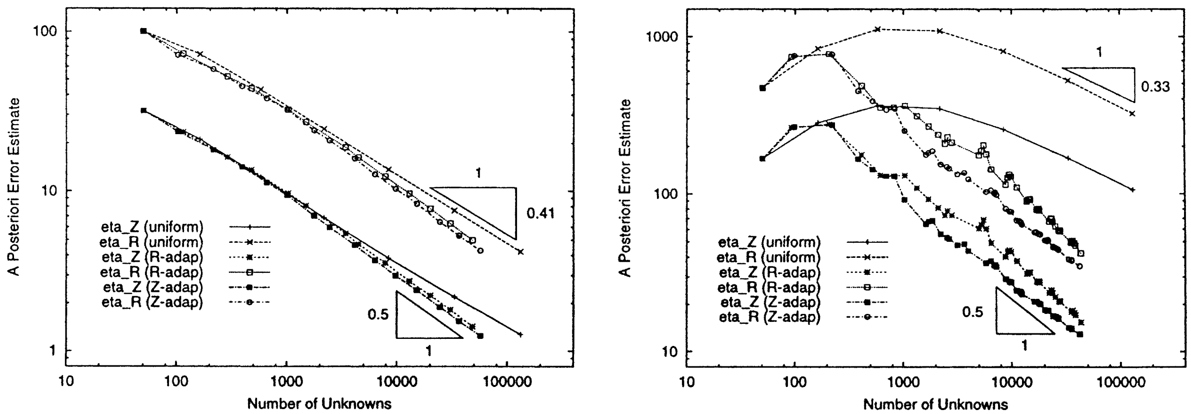

Fig. 7. Error indicators $\eta_{\mathscr{A}}$ and η_R vs N for uniform and adaptive meshes from Algorithm $(A^0_{\mathscr{A}})$ and (A^0_R) of Section 4.2 ($\nu = 1/3$ left, $\nu = 0.499$ right.)

For $\mu = 1/3$, 0.499 and all values of N corresponding to $\mathscr{T}_1, \ldots, \mathscr{T}_k$ implicitly shown in Fig. 7 we calculate $2.63 \leqslant \eta_R/\eta_{\mathscr{A}} \leqslant 3.6$; the behaviour of the error estimators η_R and $\eta_{\mathscr{A}}$ is the same with respect to λ. In contrast, the quotient $\eta_R/\eta_{\mathscr{A}}$ seems to be unbounded as λ and $\max(h_{\mathscr{T}})^{-1}$ increase for the error indicators η_R and $\eta_{\mathscr{A}}$ in Part I [6] (c.f. [6, Section 4.3]).

By Algorithm $(A^0_{\mathscr{A}})$ we obtain meshes with slightly smaller quantities η_R and η_Z than those generated by Algorithm (A^0_Z) and to reach a given tolerance Algorithm (A^0_R) needs more adaptive iterations than $(A^0_{\mathscr{A}})$.

4.3. Compact tension specimen

The compact tension specimen of Fig. 8 is loaded with a surface load $g = (0, 100)$ on $\Gamma_N = \{(x, y) \in \Gamma : |y| = 60\}$ and $f = 0$; $E = 100,000$ and $\nu = 1/3$ and 0.4999. The specimen is subjected to a vertical elongation. As the problem is symmetric, one half of the domain was discretised. We fixed the horizontal displacement with the constraint that the integral mean of all horizontal displacements is zero.

For coarse meshes, the problem behaves like a problem with re-entrant corner at $A = (50, 0)$ and hence we expect a higher mesh-refinement. The numerical solution for this problem with $\nu = 1/3$ and $N = 21,503$ and a magnification of the adaptively refined mesh around $(50, 0)$ is provided in Fig. 8. The a posteriori error estimates $\eta_{\mathscr{A}}$ and η_R are plotted versus the number of degrees of freedom N in Fig. 9 (see Fig. 10). Assuming efficiency and reliability constants as computed in Section 4.1 we obtain optimal convergence

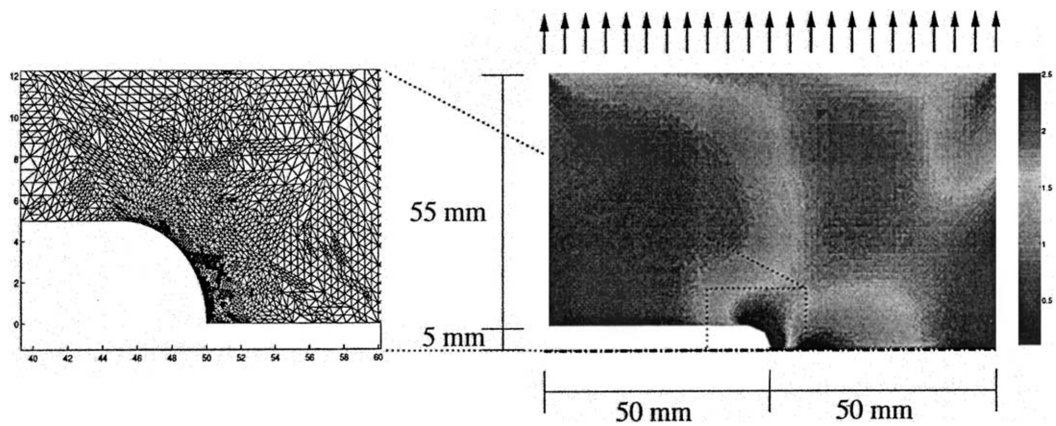

Fig. 8. Plot of the approximated von-Mises stress after 11 refinements generated by Algorithm $(A^0_{\mathscr{A}})$ and magnified detail at $(50, 0)$ of Section 4.3 ($\nu = 1/3$).

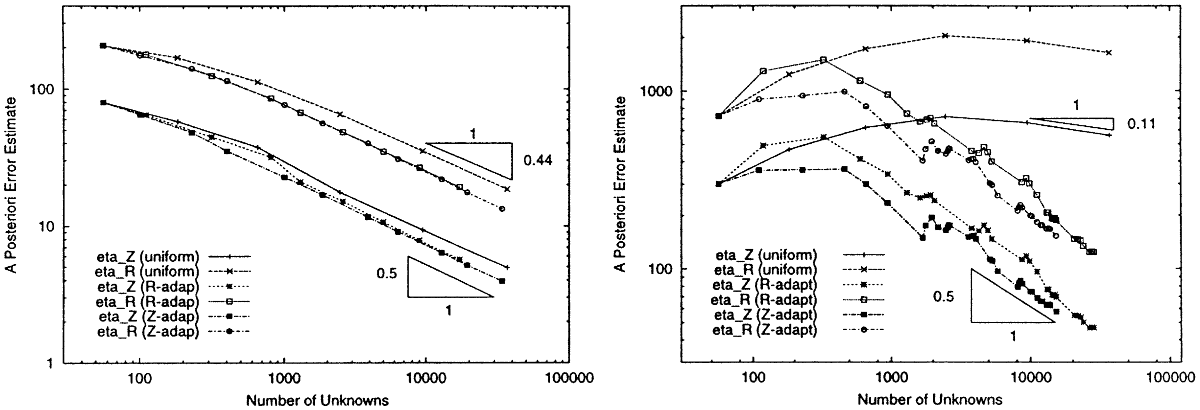

Fig. 9. Error indicators $\eta_{\mathscr{A}}$ and η_R vs N for uniform and adaptive meshes from Algorithm $(A^0_{\mathscr{A}})$ and (A^0_R) of Section 4.3 ($\nu = 1/3$ left, $\nu = 0.499$ right).

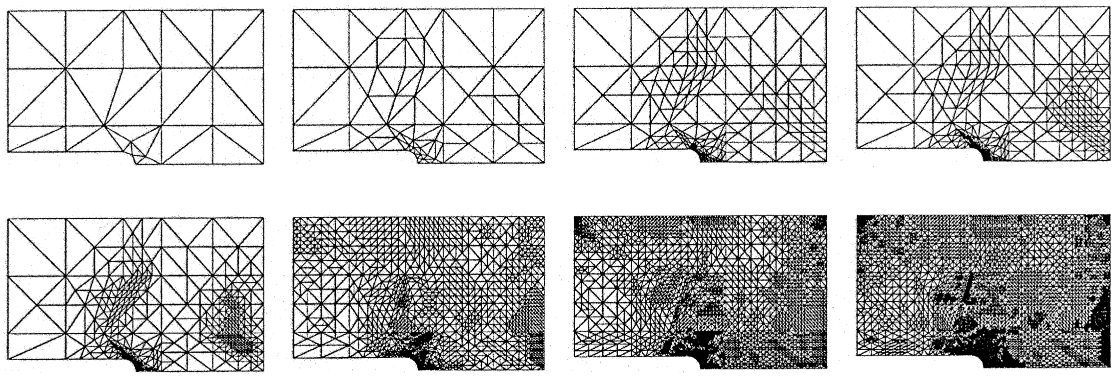

Fig. 10. $\mathscr{T}_0, \ldots, \mathscr{T}_7$ generated by Algorithm $(A^1_{\mathscr{A}})$ in Section 4.3 ($\nu = 1/3$).

rates 1 of e_N for adaptive meshes. The convergence rate of $\eta_{\mathscr{A}}$ and η_R is approximately 1 for the adaptive meshes and (computed from the last two meshes) 0.44, resp. 0.11 for uniform meshes.

Both adaptive mesh-refining Algorithms $(A^0_{\mathscr{A}})$ and (A^0_R) improve this experimental convergence order to the optimal order one. Similar as in Section 4.2 we get $2.6 \leqslant \eta_R/\eta_{\mathscr{A}} \leqslant 3.45$ for all calculated examples.

5. Proofs

Let u solve (2.1)–(2.4), respectively, let u_h satisfy (2.7). Then define the exact and discrete pressure

$$p := -\lambda \operatorname{div} u \quad \text{and} \quad p_h := \lambda \operatorname{div} u_h \tag{5.1}$$

such that the stress–strain relations read

$$\sigma = 2\mu\varepsilon(u) - p\mathbb{1} \quad \text{and} \quad \sigma_h = 2\mu\varepsilon(u_h) - p_h\mathbb{1}. \tag{5.2}$$

For brevity, we define the errors

$$e := u - u_h \in H^1(\Omega)^d \quad \text{and} \quad \delta := p - p_h \in L^2(\Omega) \tag{5.3}$$

and frequently write $\|\cdot\|_{2,\Omega} := \|\cdot\|_{L^2(\Omega)}$ and $\|\cdot\|_{1,2,\Omega} := \|\cdot\|_{H^1(\Omega)}$ and in this notation even neglect the domain Ω if there is no risk of confusion.

In the first step of the proof, We consider an auxiliary variable to control δ in the sequel. Notice that we need the extra condition $\int_\Omega \delta \,\mathrm{d}x = 0$ in case $\Gamma = \Gamma_\mathrm{D}$ which then is equivalent to (2.8).

Lemma 5.1 [3,6]. *There exist a constant $c_8 = c_8(\Omega, \Gamma_\mathrm{N})$ and a function $w \in H^1_\mathrm{D}(\Omega) := \{v \in H^1(\Omega)^d : v = 0$ on $\Gamma_\mathrm{D}\}$ with*

$$\operatorname{div} w = \delta \qquad \text{and} \qquad ||w||_{H^1(\Omega)} \leqslant c_8 ||\delta||_{L^2(\Omega)} \qquad \square. \tag{5.4}$$

Similar to [6] we employ w to define some function

$$v := 2\mu\ c_8^2 e - w \in H^1(\Omega)^d. \tag{5.5}$$

Lemma 5.2. *We have*

$$2\mu^2 c_8^2 ||\varepsilon(e)||^2_{L^2(\Omega)} + (1/2 + 2\mu c_8^2/\lambda)||\delta||^2_{L^2(\Omega)} \leqslant \int_\Omega (\sigma - \sigma_h) : \varepsilon(v)\,\mathrm{d}x. \tag{5.6}$$

Proof. A direct calculation (merely employing the definitions in (5.1), (5.2) and (5.5) yields

$$4\mu^2 c_8^2 ||\varepsilon_{\mathcal{T}}(e)||_2^2 + (1 + 2\mu c_8^2/\lambda)||\delta||_2^2 = \int_\Omega (\sigma - \sigma_h) : \varepsilon(v)\,\mathrm{d}x + 2\mu \int_\Omega \varepsilon(e) : \varepsilon(w)\,\mathrm{d}x. \tag{5.7}$$

Employing (5.4), Cauchy's, and Young's inequalities we deduce

$$2\mu \int_\Omega \varepsilon(e) : \varepsilon(w)\,\mathrm{d}x \leqslant 2\mu^2 c_8^2 ||\varepsilon(e)||_2^2 + \frac{1}{2}||\delta||_2^2. \tag{5.8}$$

A combination of (5.7) and (5.8) shows the assertion (5.6). $\square$

The subsequent approximation operator is the key to our reliability proof of the averaging techniques for error control. The set of free nodes is $\mathcal{K} := \mathcal{N} \setminus \Gamma_\mathrm{D}$ and for each node Ω_z is a (possibly enlarged) patch (i.e., union of neighbouring elements) of diameter h_z [4,5].

Lemma 5.3 [4,5,9]. *There exists a linear mapping $\mathcal{J} : H^1_\mathrm{D}(\Omega) \to \mathcal{S}$ which satisfies*

$$||\nabla \mathcal{J}\varphi||_{L^2(\Omega)} + ||h_{\mathcal{T}}^{-1}(\varphi - \mathcal{J}\varphi)||_{L^2(\Omega)} + ||h_{\mathcal{E}}^{-1/2}(\varphi - \mathcal{J}\varphi)||_{L^2(\cup\mathcal{E})}) \leqslant c_9 ||\nabla\varphi||_{L^2(\Omega)} \tag{5.9}$$

for all $\varphi \in H^1_\mathrm{D}(\Omega)$. In addition, there holds for all $R \in L^2(\Omega)^d$

$$\int_\Omega R \cdot (\varphi - \mathcal{J}\varphi)\,\mathrm{d}x \leqslant c_{10} ||\nabla\varphi||_{L^2(\Omega)} \left(\sum_{z \in \mathcal{K}} h_z^2 \min_{R_z \in \mathbb{R}^d} \int_{\Omega_z} |R - R_z|^2\,\mathrm{d}x \right)^{1/2}. \tag{5.10}$$

The positive constants c_9, c_{10} do not depend on the mesh-sizes $h_{\mathcal{T}}$ and $h_{\mathcal{E}}$, but on the shape of the elements only. $\square$

Proof of Theorem 2.1. Because of Lemma 5.2 and with some η as in (2.9), we focus on the term

$$\int_\Omega (\sigma - \sigma_h) : \varepsilon(v)\,\mathrm{d}x = 2\mu c_8^2 \int_\Omega (\sigma - \sigma_h) : \varepsilon(\eta - u_h)\,\mathrm{d}x + \int_\Omega (\sigma - \sigma_h) : \varepsilon(z - \mathcal{J}z)\,\mathrm{d}x, \tag{5.11}$$

when $z := 2\mu c_8^2(u - \eta) - w$ and we employed (2.7) for $v_h = \mathcal{J}z$. This and Lemma 5.2 show

$$||2\mu\varepsilon(e)||^2_{L^2(\Omega)} + ||\delta||^2_{L^2(\Omega)} \leqslant c_{11} \left(\eta_\mathrm{D}^2 + \int_\Omega (\sigma - \sigma_h) : \varepsilon(z - \mathcal{J}z)\,\mathrm{d}x \right) \tag{5.12}$$

A $\mathcal{T}$-elementwise integration by parts and a reorganisation of all the boundary term on $\cup\mathcal{E}$ (cf. [14,15] for details) with the volume residual $R := f + \operatorname{div}_{\mathcal{T}}\sigma_h = f$ and the stress jumps J yield

$$\int_\Omega (\sigma - \sigma_h) : \varepsilon(z - \mathcal{J}z)\,\mathrm{d}x = \int_\Omega R \cdot (z - \mathcal{J}z)\,\mathrm{d}x - \int_{\cup\varepsilon} J \cdot (z - \mathcal{J}z)\,\mathrm{d}s. \tag{5.13}$$

Lemma 5.3 and a few applications of Cauchy's inequality prove, with $R_z \in \mathbb{R}^d$ for $z \in \mathcal{K}$,

$$\int_\Omega (\sigma - \sigma_h) : \varepsilon(z - \mathcal{J}z)\,\mathrm{d}x \leqslant \left(c_{10} \left(\sum_{z\in\mathcal{K}} h_z^2 ||R - R_z||^2_{2,\Omega_z} \right)^{1/2} + c_9 ||h_{\mathcal{E}}^{1/2} J||_{2,\cup\mathcal{E}} \right) ||\nabla_z||_2. \tag{5.14}$$

By Korn's inequality, the definitions of z, η_D and because of (5.4)

$$||\nabla_z||_2 \leqslant c_{12} ||\varepsilon(z)||_2 \leqslant c_{13}(||2\mu\varepsilon(e)||_2 + \eta_\mathrm{D} + ||\delta||_2). \tag{5.15}$$

Thus, Young's inequality shows in (5.14) that

$$\int_\Omega (\sigma - \sigma_h) : \varepsilon(z - \mathcal{J}z)\,\mathrm{d}x \leqslant \frac{1}{2} ||2\mu\varepsilon(e)||^2_{L^2(\Omega)} + \frac{1}{2} ||\delta||^2_{L^2(\Omega)} + c_{14} \left(||h_{\mathcal{E}}^{1/2} J||^2_{2,\cup\mathcal{E}} + \eta_\mathrm{D}^2 + \sum_{z\in\mathcal{K}} h_z^2 ||R - R_z||^2_{2,\Omega_z} \right). \tag{5.16}$$

The assertion of Theorem 2.1 follows from (5.12) and (5.16) when we set $R_z = 0$. □

Proof of Theorem 2.2. Coming back to (5.16) but choosing R_z as the integral mean of $R = f$ on Ω_z and Poincaré inequality show $||R - R_z||_{2,\Omega_z} \leqslant C(\Omega_z)||\nabla f||_{2,\Omega_z}$ where $C(\Omega_z)/h_z$ depends on the shape of the patch only. Then, for each element $T \subset \overline{\Omega}_z$, $C(\Omega_z)/h_T$ is $h_{\mathcal{T}}$-independent and depends on the aspect ratio of the elements only. This, and the fact that the patches have a finite overlap show that

$$\sum_{z\in\mathcal{K}} ||R - R_z||^2_{2,\Omega_z} \leqslant c_{15} ||h_{\mathcal{T}}^2 \nabla f||_2^2. \tag{5.17}$$

Utilising (5.17) in (5.16), the assertion of Theorem 2.2 follows from (5.12).

Proof of Theorem 2.4. Coming back to (5.16) we follow the lines of the proof in Part I (cf. (5.9)–(5.12) in [6] with w instead of z) to verify

$$\int_\Omega (\sigma - \sigma_h) : \varepsilon(z - \mathcal{J}z)\,\mathrm{d}x \leqslant c_{16}^{-1} ||\nabla_z||_2 \left(||\sigma_h - \sigma_h^*||_{L^2(\Omega)} + ||h^{3/2\varepsilon} \partial_{\mathcal{E}} g/\partial s||_{L^2(\Gamma_\mathrm{N})} + ||h_{\mathcal{T}}^2 \nabla f||_{L^2(\Omega)} \right). \tag{5.18}$$

This, (5.12) and (5.15) prove the assertion.

References

[1] I. Babuška, W.C.R. Rheinboldt, Error estimates for adaptive finite element computations, SIAM J. Numer. Anal. 15 (1978) 736–754.

[2] S. Bartels, C. Carstensen, Each Averaging technique yields reliable a posteriori error control in FEM on unstructured grids. Part II: Higher order FEM Berichtsreihe des Mathematischen Seminars der Universität Kiel, Technical Report 00-5, Christian-Albrechts-Universität zu Kiel, Kiel, 2000. http://www.numerik.uni-kiel.de/reports/2000/00-5.html.

[3] F. Brezzi, M. Fortin, Mixed and Hybrid Finite Element Methods, Springer, Berlin, 1991.

[4] C. Carstensen, Quasi interpolation and a posteriori error analysis in finite element method, M^{2}AN 33 (1999) 1187–1202.

[5] C. Carstensen, S. Bartels, Each averaging technique yields reliable a posteriori error control in FEM on unstructured grids Part I: low order conforming, non-conforming and mixed FEM, Berichtsreihe des Mathematischen Seminars Kiel, Technical Report 99-11, Christian-Albrechts-Universität zu Kiel, Kiel, 1999. http://www.numerik.uni-kiel.de/reports/1999/99-11.html.

[6] C. Carstensen, S.A. Funken, Averaging technique for FE-a posteriori error control in elasticity. Part I: Conforming FEM Berichtsreihe des Mathematischen Seminars Kiel, Technical report 99-14, Christian-Albrechts-Universität zu Kiel, Kiel, 1999. http://www.numerik.uni-kiel.de/reports/1999/99-14.html.

[7] C. Carstensen, S.A. Funken, Averaging technique for FE-a posteriori error control in elasticity. Part III: Locking-free FEM Berichtsreihe des Mathematischen Seminars der Universität Kiel, Technical Report 00-11, Christian-Albrechts-Universität zu Kiel, Kiel 2000. Compat. Methods Appl. Mech. Engrg. (accepted) http://www.numerik.uni-kiel.de/reports/2000/00-11.html.

[8] C. Carstensen, S.A. Funken, A posteriori error control in low-order finite element discretisations on incompressible stationary flow problems Berichtsreihe des Mathematischen Seminars Kiel, Technical Report 99-5, Christian-Albrechts-Universität zu Kiel, Kiel, 1999, Math. Comp. (accepted). http://www.numerik.uni-kiel.de/reports/1999/99-5.html.
[9] C. Carstensen, R. Verfürth, Edge residuals dominate a posteriori error estimates for low order finite element methods. Berichtsreihe des Mathematischen Seminars Kiel, Technical Report 97-6 Christian-Albrechts-Universität zu Kiel, SIAM J. Numer. Anal. 36 (1998) 1571–1587.
[10] P.G. Ciarlet, The Finite Element Method for Elliptic Problems, North-Holland, Amsterdam, 1978.
[11] K. Eriksson, D. Estep, P. Hanspo, C. Johnson, Introduction to adaptive methods for differential equations, Acta Numerica (1995) 105–158.
[12] L. Hörmander, Linear Partial Differential Operators, Springer, Berlin, Heidelberg, New York, 1963.
[13] J.L. Lions, E. Magenes, Non-homogeneous Boundary Value Problems and Applications, vol. 1, Springer, Berlin, 1972.
[14] R. Verfürth, A Review of Posteriori Error Estimation and Adaptive Mesh-Refinement Techniques, Wiley, New York, 1996.
[15] R. Verfürth, A review of a posteriori error estimation techniques for elasticity problems, in: P. Ladevze, J.T. Oden (Eds.), On New Advances in adaptive Computational Methods in Mechanics, Elsevier, Amsterdam, 1997.
[16] O.C. Zienkiewicz, J.Z. Zhu, A simple error estimator and adaptive procedure for practical engineering analysis, Int. J. Numer. Meth. Engrg. 24 (1987) 337–357.